Palestine Journal of Mathematics

Vol. 8(1)(2019) , 8–22 © Palestine Polytechnic University-PPU 2019

MHD Pulsatile flow of a Micropolar fluid sandwiched between viscous fluids inside permeable beds: An analytical study.

Manju Agarwal and Deepak Kumar*

Communicated by S. Khuri

MSC 2010 Classifications: Primary 76S99; Secondary 76T99.

Keywords and phrases: Pulsatile flow, Micropolar fluid, Immiscible fluids, Permeable bed, Beaver-Joseph slip boundary condition.

Abstract The paper deals with the MHD pulsating flow of a micropolar fluid, sandwiched between two viscous fluid layers inside permeable beds. Flow is considered in three Regions: Region I and Region III contain the flow of Newtonian fluids while Region II includes the flow of an electrically conducting micropolar fluid. Flow in Regions, I and III are assumed to be governed by Navier-stokes equation and in Region II by constitutive equations proposed by Eringen[16]. Continuity of velocity and shear stress is imposed at the fluid-fluid interface and B-J slip boundary condition is employed at the fluid porous interface. The governing equations are solved analytically and the expressions for velocity, mass flux, and shear stress are obtained. The effects of physical governing parameters on velocity and shear stress on the permeable beds are investigated.

1 Introduction

Study of multiphase flow has been one of the areas of great current interest due to increasing applications. Examples of these applications are in the field of agricultural engineering to study underground water resources[1]; in the petroleum industry to study the movement of natural gases, oil and water through oil reservoirs; in studies of water in river beds. The term multiphase flow refers to the flow of two or more immiscible fluids of different densities/viscosities in the same channel or through porous media. Blood flow in arteries has been studied by many researchers considering blood as a two-phase flow[2, 3, 4, 5].

Vajravelu et al.[6] studied the hydromagnetic unsteady flow of two conducting immiscible fluids between two permeable beds. After that, they analysed the pulsatile flow of a viscous fluid between two permeable beds[7]. Flow inside permeable beds, under exponentially decaying pressure gradient is investigated by Prasad and Kumar[8]. Jogie and Bhatt[9] studied the flow of immiscible fluids in a naturally permeable channel using B-J slip condition. Srinivas and Murthy[10] studied the flow of two immiscible couple stress fluids between permeable beds and concluded that presence of the couple stress reduces flow velocity. Three-layer fluid flow over a small obstruction on the bottom of a channel is studied by S. Panda et.al.[11]. Umavathi et.al.[12] studied unsteady flow in the porous medium sandwiched between viscous fluids. In the case of flow past porous medium, Beavers and Joseph[13] have shown that the usual no-slip boundary condition is no longer valid for porous boundaries and postulated the existence of slip at the interface of a porous boundary resulting in the condition called B-J slip condition. According to this condition, the Poiseuille velocity in a channel and Darcy's velocity in the porous medium can be coupled through the following equation:

$$\frac{\partial u_f}{\partial y} = \frac{\alpha}{K^{\frac{1}{2}}}(u_f - u_m)$$

Here the clear fluid region occupies the region ($y > 0$), u_f is the fluid velocity and u_f and $\frac{\partial u_f}{\partial y}$ are evaluated at $y = 0+$. The Darcy velocity u_m is evaluated at some small distance below from $y = 0$. The Beaver-Joseph constant α is dimensionless constant, depends on the structure of porous medium and independent of the fluid viscosity.

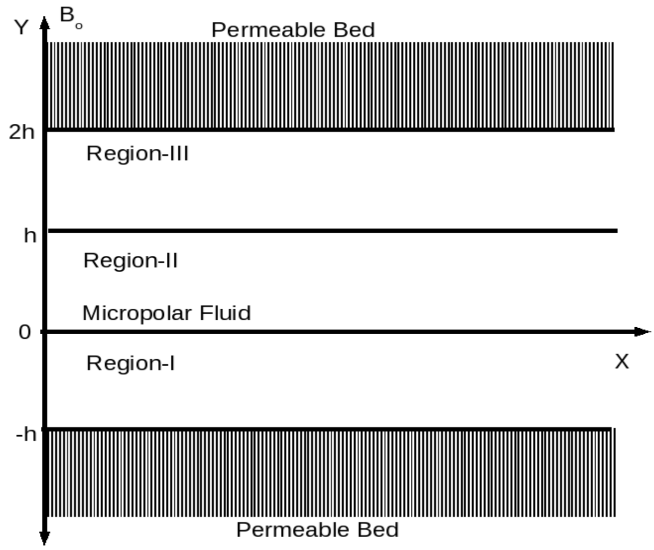

Figure 1

In recent years an enormous research is done on the flow of micro fluids as this class of fluids represents many important fluids like paints, polymer, suspension and colloid fluids. Blood flow is modelled as micropolar fluid flow by many authors[14, 15]. The micropolar fluid model, introduced by Eringen[16, 17] is an extension of classical fluid dynamics. It takes into account microrotation to the molecules different from the local vorticity of the flow. The occurrence of microrotation vector which differs from the stream flow vorticity and angular velocity results into formation of antisymmetric stress and couple stresses. Early studies and application of micropolar fluid mechanics can be found in the review article by Peddieson and McNitt[18], and Ariman et al.[19] and in the recent books by Lukaszewicz [20] and Eringen [21].

In past years, a significant research has been done on the flow of micropolar fluids. Effect of induced magnetic field on a peristaltic flow of micropolar fluid is analysed by Kh. S. Mekheimer[22]. Bitla and Iyenger[23] studied pulsating flow of an incompressible micropolar fluid between permeable beds. An analytical solution to the MHD flow of micropolar fluid over a linearly stretching sheet is obtained by Siddheshwar and Mahabaleshwar[24]. Prathap Kumar et.al.[25] studied the fully-developed free convective flow of micropolar and viscous fluids in a vertical channel. Rawat et.al.[26] analysed MHD flow and heat transfer of micropolar fluid of variable micro inertia density in a porous medium. Flow and heat transfer of two micropolar fluids separated by a viscous fluid layer is investigated by Umavathi et al. [27]. Umavathi et.al.[28] also analysed flow and heat transfer of a micropolar fluid sandwiched between viscous fluid layers.

In view of various applications of MHD pulsating flow of micropolar fluids in natural systems, human systems and in many engineering problems, we analyzed an MHD pulsating flow of a micropolar fluid, sandwiched between two viscous fluid layers inside permeable beds.The effects of different flow parameters on velocity are displayed graphically and that on shear stress at permeable beds are presented numerically through tables.

2 Mathematical Formulation

The geometry under consideration is illustrated in Fig. 1, consists of a region inside the permeable beds. The region $0 \leq y \leq h$ is occupied by a micropolar fluid of density ρ_2, viscosity μ_2 and vortex viscosity k, the region $-h \leq y \leq 0$ is filled with a viscous fluid of density ρ_1 and viscosity μ_1. Region $h \leq y \leq 2h$ is also filled by a viscous fluid of density ρ_3 and viscosity μ_3.

The field equations describing a micropolar fluid[16] are given by

$$\frac{\partial \rho}{\partial t} = div(\rho \vec{V}) \tag{2.1}$$

$$\rho \frac{d\vec{V}}{dt} = \rho \vec{f} - gradp + kcurl\vec{v} - (\mu + k)curl(curl\vec{V}) + (\lambda + 2\mu + k)grad(div\vec{V}) \tag{2.2}$$

$$\rho j \frac{d\vec{v}}{dt} = \rho \vec{l} - 2k\vec{v} + Kcurl\vec{V} - \gamma curl(curl\vec{v}) + (\alpha' + \beta + \gamma)grad(div\vec{v}) \tag{2.3}$$

where $\vec{V}$ and $\vec{v}$ are velocity and microrotation vectors, respectively. $\vec{f}$, $\vec{l}$ are the body force per unit mass, body couple per unit mass respectively, and p is the pressure at any point. ρ and j are the density of the fluid and microinertia density respectively, and are assumed to be constant. The material quantities (λ, μ, k) are viscosity coefficients and (α', β, γ) are gyroviscosity coefficients satisfying the constraints

$$k \geq 0, (2\mu + k) \geq 0, (3\lambda + 2\mu + k) \geq 0, \gamma \geq 0, \beta \geq 0, (3\alpha' + \beta + \gamma) \geq 0$$

Equations $(2.1) - (2.3)$ represent the conservation of mass, conservation of linear momentum and conservation of micro-inertia respectively. In the absence of $\vec{l}$, $\vec{f}$ and $k = \alpha' = \beta = \gamma = 0$, microrotation (gyration) vector becomes zero and the governing equations reduce to Navier-Stokes equations.

We consider the fluids to be incompressible and immiscible and the flow is unsteady, laminar and fully developed and driven only by a pulsatile pressure gradient

$$\frac{\partial p}{\partial x} = \left(\frac{\partial p}{\partial x}\right)_s + \left(\frac{\partial p}{\partial x}\right)_o e^{iwt}$$

where $\left(\frac{\partial p}{\partial x}\right)_s$ and $\left(\frac{\partial p}{\partial x}\right)_o$ are amplitudes of steady and oscillatory pulsations respectively and w is the frequency. It is noted that the viscous fluids and micropolar fluid are immiscible (that is there exist no mixing between the fluids) and the constitutive equations for viscous fluids and micropolar fluid are different. For instance, Synovial fluid which is a clear thixotropic lubrication fluid is a good example of micropolar fluids and water is a good example for viscous fluids and it is well known that a synovial fluid and water can not mixed. Since our model is general, One can choose any different fluids which are immiscible.

Assuming that non-zero component of velocity is X-component and in the absence of body forces and body couple, the governing equations of fluid flow are

Region-I

$$\rho_1 \frac{\partial u_1}{\partial t} = -\frac{\partial p}{\partial x} + \mu_1 \frac{\partial^2 u_1}{\partial y^2} \tag{2.4}$$

Region-II

$$\rho_2 \frac{\partial u_2}{\partial t} = -\frac{\partial p}{\partial x} + (\mu_2 + k)\frac{\partial^2 u_2}{\partial y^2} + k\frac{\partial c}{\partial y} - \sigma B_o^2 u_2 \tag{2.5}$$

$$\rho_2 j \frac{\partial c}{\partial t} = -2kc - k\frac{\partial u_2}{\partial y} + \gamma \frac{\partial^2 c}{\partial y^2} \tag{2.6}$$

Region-III

$$\rho_3 \frac{\partial u_3}{\partial t} = -\frac{\partial p}{\partial x} + \mu_3 \frac{\partial^2 u_3}{\partial y^2} \tag{2.7}$$

Here k, γ and j are vortex viscosity, spin gradient viscosity and microinertia density. σ is electrical conductivity of micropolar fluid and B_o is strength of applied magnetic field, in direction normal to the flow.

Herein the velocities $u_1(y,t), u_2(y,t), u_3(y,t)$ and microrotation velocity $c(y,t)$ is to satisfy the conditions

$$\frac{\partial u_1}{\partial y} = \frac{\alpha}{\sqrt{K_1}}(u_1' - Q_1) \qquad \text{at } y = -h \tag{2.8}$$

$$u_1' = u_1 \qquad \text{at } y = -h \tag{2.9}$$

$$\mu_1 \frac{\partial u_1}{\partial y} = (\mu_2 + k)\frac{\partial u_2}{\partial y} + kc \qquad \text{at } y = 0 \tag{2.10}$$

$$c = 0 \qquad \text{at } y = 0 \tag{2.11}$$

$$u_1 = u_2 \qquad \text{at } y = 0 \tag{2.12}$$

$$\mu_3 \frac{\partial u_3}{\partial y} = (\mu_2 + k)\frac{\partial u_2}{\partial y} + kc \qquad \text{at } y = h \tag{2.13}$$

$$c = 0 \qquad \text{at } y = h \tag{2.14}$$

$$u_2 = u_3 \qquad \text{at } y = h \tag{2.15}$$

$$\frac{\partial u_3}{\partial y} = -\frac{\alpha}{\sqrt{K_2}}(u_3' - Q_2) \qquad \text{at } y = 2h \tag{2.16}$$

$$u_3' = u_3 \qquad \text{at } y = 2h \tag{2.17}$$

Where $Q_1 = -\frac{K_1}{\mu_1}\frac{\partial p}{\partial x}$ and $Q_2 = -\frac{K_2}{\mu_3}\frac{\partial p}{\partial x}$ are Darcy's velocities in the upper and lower permeable beds. Equations (2.8&2.16) represent the B-J slip boundary conditions respectively, at the interfaces of upper and lower permeable beds. Equations (2.11&2.14) stipulates that the microrotation velocity vanishes at the interfaces of the viscous fluids. In view of the pulsating pressure gradient, let us assume that the velocities and microrotation velocity are in the form

$$u_i = u_{i1} + u_{i2}e^{iwt}, \qquad i = 1, 2, 3$$
$$c = c_s + c_o e^{iwt}$$

where u_{i1} and c_s represent steady parts and u_{i2} and c_o represent the oscillatory parts of the velocity and microrotation respectively.

3 Non-dimensionalization of flow quantities

We introduce following non dimensional quantities to make the governing equations and the boundary conditions dimensionless:

$$x^* = \frac{x}{h}, y^* = \frac{y}{h}, u_i^* = \frac{u_i}{u}, u_{i1}^* = \frac{u_{i1}}{u},$$
$$u_{i2}^* = \frac{u_{i2}}{u}, c^* = \frac{c}{h}, c_s^* = \frac{c_s}{h}, c_o^* = \frac{c_o}{h},$$
$$t^* = \frac{tu}{h}, K_i^* = \frac{K_i}{h^2}, w^* = \frac{wh}{u}, p^* = \frac{p}{\rho u^2}$$

After dropping the asterisks, governing equations of motion (2.4, 2.5, 2.6, 2.7) are given by

$$\frac{\partial u_1}{\partial t} = -\frac{\partial p}{\partial x} + \frac{1}{R_1}\frac{\partial^2 u_1}{\partial y^2} \tag{3.1}$$

$$\frac{\partial u_2}{\partial t} = -\rho\frac{\partial p}{\partial x} + \frac{1}{R_2}\frac{\partial^2 u_2}{\partial y^2} + \frac{C_p}{R_2}\frac{\partial c}{\partial y} - \frac{M^2}{R_2}u_2 \tag{3.2}$$

$$\frac{\partial c}{\partial t} = -\frac{2n}{R_2 P_j}c - \frac{n}{R_2 P_j}\frac{\partial u_2}{\partial y} + \frac{1}{R_2 P_j}\frac{\partial^2 c}{\partial y^2} \tag{3.3}$$

$$\frac{\partial u_3}{\partial t} = -\rho'\frac{\partial p}{\partial x} + \frac{1}{R_3}\frac{\partial^2 u_3}{\partial y^2} \tag{3.4}$$

and boundary conditions $(2.8-2.17)$ become

$$\begin{aligned}
\frac{\partial u_1}{\partial y} &= \alpha\sigma_1(u_1' + \frac{R_1}{\sigma_1^2}\frac{\partial p}{\partial x}) \qquad \text{at } y=-1 && (3.5)\\
u_1' &= u_1 \qquad \text{at } y=-1 && (3.6)\\
\frac{\mu}{m}\frac{\partial u_1}{\partial y} &= \frac{1}{C_p}\frac{\partial u_2}{\partial y} + c \qquad \text{at } y=0 && (3.7)\\
c &= 0 \qquad \text{at } y=0 && (3.8)\\
u_1 &= u_2 \qquad \text{at } y=0 && (3.9)\\
\frac{\mu'}{m}\frac{\partial u_3}{\partial y} &= \frac{1}{C_p}\frac{\partial u_2}{\partial y} + c \qquad \text{at } y=1 && (3.10)\\
c &= 0 \qquad \text{at } y=1 && (3.11)\\
u_2 &= u_3 \qquad \text{at } y=1 && (3.12)\\
\frac{\partial u_3}{\partial y} &= -\alpha\sigma_2(u_3' + \rho'\frac{R_3}{\sigma_2^2}\frac{\partial p}{\partial x}) \qquad \text{at } y=2 && (3.13)\\
u_3' &= u_3 \qquad \text{at } y=2 && (3.14)
\end{aligned}$$

where

$$\begin{aligned}
u_i &= u_{i1} + u_{i2}e^{iwt}\,, \qquad i=1,2,3\\
c &= c_s + c_o e^{iwt}\\
-\frac{\partial p}{\partial x} &= \left(\frac{\partial p}{\partial x}\right)_s + \left(\frac{\partial p}{\partial x}\right)_o e^{iwt}
\end{aligned}$$

are non-dimensional velocities, mocrorotation and pressure gradient respectively.

$M = B_o h\sqrt{\frac{\sigma}{\mu_2+k}}$ is the Hartmann's number. $R_1 = \frac{\rho_1 hu}{\mu_1}, R_2 = \frac{\rho_2 hu}{\mu_2+k}, R_3 = \frac{\rho_3 hu}{\mu_3}$ are Reynolds numbers respectively in flow regions I, II, III and $\sigma_1 = \frac{h}{\sqrt{K_1}}, \sigma_2 = \frac{h}{\sqrt{K_2}}$ are non-dimensional parameters inversely proportional to square root of permeabilities of regions $I\&III$ respectively. $C_p = \frac{k}{\mu_2+k}$ is coupling parameter. $P_j = \frac{j(\mu_2+k)}{\gamma}$ is micorotation parameter, $n = \frac{kh^2}{\gamma}$ is gyration parameter and $m = \frac{k}{\mu_2}$ is micropolar fluid material parameter.$\rho = \frac{\rho_1}{\rho_2}, \rho' = \frac{\rho_1}{\rho_3}, \mu = \frac{\mu_1}{\mu_2}$ and $\mu' = \frac{\mu_3}{\mu_2}$ are non-dimensional parameters.

3.1 Steady flow

The governing equations of steady flow are given by

$$\begin{aligned}
\frac{d^2u_{11}}{dy^2} + R_1 P_s &= 0 && (3.15)\\
\frac{d^2u_{21}}{dy^2} + C_p\frac{\partial c_s}{\partial y} - M^2u_{21} + \rho R_2 P_s &= 0 && (3.16)\\
\frac{d^2c_s}{dy^2} - n\frac{du_{21}}{dy} - 2nc_s &= 0 && (3.17)\\
\frac{d^2u_{31}}{dy^2} + \rho' R_3 P_s &= 0 && (3.18)
\end{aligned}$$

The boundary conditions to be satisfied by u_{i1} & c_s are

$$\frac{du_{11}}{dy} = \alpha\sigma_1(u'_{11} - \frac{R_1}{\sigma_1^2}P_s) \qquad \text{at } y = -1 \tag{3.19}$$

$$u'_{11} = u_{11} \qquad \text{at } y = -1 \tag{3.20}$$

$$\frac{\mu}{m}\frac{du_{11}}{dy} = \frac{1}{C_p}\frac{du_{21}}{dy} + c_s \qquad \text{at } y = 0 \tag{3.21}$$

$$c_s = 0 \qquad \text{at } y = 0 \tag{3.22}$$

$$u_{11} = u_{21} \qquad \text{at } y = 0 \tag{3.23}$$

$$\frac{\mu'}{m}\frac{du_{31}}{dy} = \frac{1}{C_p}\frac{du_{21}}{dy} + c_s \qquad \text{at } y = 1 \tag{3.24}$$

$$c_s = 0 \qquad \text{at } y = 1 \tag{3.25}$$

$$u_{21} = u_{31} \qquad \text{at } y = 1 \tag{3.26}$$

$$\frac{du_{31}}{dy} = -\alpha\sigma_2(u'_{31} - \rho'\frac{R_3}{\sigma_2^2}P_s) \qquad \text{at } y = 2 \tag{3.27}$$

$$u'_{31} = u_{31} \qquad \text{at } y = 2 \tag{3.28}$$

where $P_s = (\frac{\partial p}{\partial x})_s$.

3.2 Oscillatory flow

The governing equations of oscillatory flow are given by

$$\frac{d^2u_{12}}{dy^2} - iwR_1u_{12} + R_1P_o = 0 \tag{3.29}$$

$$\frac{d^2u_{22}}{dy^2} - (M^2 + R_2iw)u_{22} + C_p\frac{dc_o}{dy} + \rho R_2P_o = 0 \tag{3.30}$$

$$\frac{d^2c_o}{dy^2} - n\frac{du_{22}}{dy} - (2n + R_2P_jiw)\,c_o = 0 \tag{3.31}$$

$$\frac{d^2u_{32}}{dy^2} - iwR_3u_{32} + \rho'R_3P_o = 0 \tag{3.32}$$

The boundary conditions to be satisfied by u_{i2} & c_o are

$$\frac{du_{12}}{dy} = \alpha\sigma_1(u'_{12} - \frac{R_1}{\sigma_1^2}P_o) \qquad \text{at } y = -1 \tag{3.33}$$

$$u'_{12} = u_{12} \qquad \text{at } y = -1 \tag{3.34}$$

$$\frac{\mu}{m}\frac{du_{12}}{dy} = \frac{1}{C_p}\frac{du_{22}}{dy} + c_o \qquad \text{at } y = 0 \tag{3.35}$$

$$c_o = 0 \qquad \text{at } y = 0 \tag{3.36}$$

$$u_{12} = u_{22} \qquad \text{at } y = 0 \tag{3.37}$$

$$\frac{\mu'}{m}\frac{du_{32}}{dy} = \frac{1}{C_p}\frac{du_{22}}{dy} + c_o \qquad \text{at } y = 1 \tag{3.38}$$

$$c_o = 0 \qquad \text{at } y = 1 \tag{3.39}$$

$$u_{22} = u_{32} \qquad \text{at } y = 1 \tag{3.40}$$

$$\frac{du_{32}}{dy} = -\alpha\sigma_2(u'_{32} - \rho'\frac{R_3}{\sigma_2^2}P_o) \qquad \text{at } y = 2 \tag{3.41}$$

$$u'_{32} = u_{32} \qquad \text{at } y = 2 \tag{3.42}$$

where $P_o = (\frac{\partial p}{\partial x})_o$.

4 Solution of the problem

4.1 Steady flow solution

The solution of steady flow described in section 3.1 is given by

$$
\begin{aligned}
u_{11} &= C_1 + C_2 y - \frac{1}{2} R_1 P_s y^2 \\
u_{21} &= C_3 e^{\lambda_1 y} + C_4 e^{\lambda_2 y} + C_5 e^{\lambda_3 y} + C_6 e^{\lambda_4 y} + \frac{R_2 P_s \rho}{M^2} \\
c_s &= D_3 e^{\lambda_1 y} + D_4 e^{\lambda_2 y} + D_5 e^{\lambda_3 y} + D_6 e^{\lambda_4 y} \\
u_{31} &= C_7 + C_8 y - \frac{1}{2} R_3 P_s \rho' y^2
\end{aligned}
$$

Since the expressions are very cumbersome so the constants $C_i, i = 1, 2, 3, 4, 5, 6, 7, 8$ and $D_j, j = 3, 4, 5, 6$ are not reported.

4.2 Oscillatory flow solution

The solution of oscillatory flow described in section 3.2 is given by

$$
\begin{aligned}
u_{12} &= C_9 e^{\sqrt{i\omega R_1} y} + C_{10} e^{-\sqrt{i\omega R_1} y} - \frac{iP_o}{\omega} \\
u_{22} &= C_{11} e^{\lambda_5 y} + C_{12} e^{\lambda_6 y} + C_{13} e^{\lambda_7 y} + C_{14} e^{\lambda_8 y} + \frac{R_2 P_o \rho}{M^2 + i\omega R_2} \\
c_o &= D_{11} e^{\lambda_5 y} + D_{12} e^{\lambda_6 y} + D_{13} e^{\lambda_7 y} + D_{14} e^{\lambda_8 y} \\
u_{32} &= C_{15} e^{\sqrt{i\omega R_3} y} + C_{16} e^{-\sqrt{i\omega R_3} y} - \frac{iP_o \rho'}{\omega}
\end{aligned}
$$

Since the expressions are very cumbersome so the constants $C_i, i = 9, 10, 11, 12, 13, 14, 15, 16$ and $D_j, j = 11, 12, 13, 14$ are not reported.

4.3 Pulsatile flow solution

The solution of pulsatile flow is given by

$$
\begin{aligned}
u_1 &= u_{11} + u_{12} e^{i\omega t} \\
u_2 &= u_{21} + u_{22} e^{i\omega t} \\
c &= c_s + c_o e^{i\omega t} \\
u_3 &= u_{31} + u_{32} e^{i\omega t}
\end{aligned}
$$

where $u_{11}, u_{21}, u_{31}, c_s$, and $u_{12}, u_{22}, c_o, u_{32}$ are reported in sections 4.1 and 4.2 respectively.

4.4 Mass flux

The instantaneous mass fluxes are given by

$$
\begin{aligned}
Q_1 &= \int_{-1}^{0} u_{11} dy + \left[\int_{-1}^{0} u_{12} dy \right] e^{i\omega t} \\
Q_2 &= \int_{0}^{1} u_{21} dy + \left[\int_{0}^{1} u_{22} dy \right] e^{i\omega t} \\
Q_3 &= \int_{1}^{2} u_{31} dy + \left[\int_{1}^{2} u_{32} dy \right] e^{i\omega t}
\end{aligned}
$$

where Q_1, Q_2 and Q_3 are mass fluxes respectively in Regions- I, II and III and full expressions are not reported due to brevity.

4.5 Shear stress

The shear stress in non-dimensional forms, at the permeable walls are given by

$$\tau_1 = \frac{\partial u_1}{\partial y} \quad \text{at } y = -1 \tag{4.1}$$

$$\tau_2 = \frac{\partial u_3}{\partial y} \quad \text{at } y = 2 \tag{4.2}$$

5 Results and Discussions

The analytical solutions for the flow velocity and microrotation of MHD pulsating flow of a micropolar fluid, sandwiched between viscous fluids inside permeable beds are obtained. The expressions are evaluated numerically for different values of governing flow parameters and presented through Figs. 2-5 and Tables 1-8. In numerical work, we take $\rho = 1, \rho' = 1$ (that is $\rho_1 = \rho_2 = \rho_3$), $\sigma_1 = \sigma_2 = \sigma$, $R_2 = \frac{\mu}{\rho} R_1$ and $R_3 = \frac{\mu}{\rho' \mu'} R_1$.

Fig. 2 shows the variation of pulsating velocity in Region-I (Fig. 2(a)), Region-II (Fig. 2(b)) and Region-III (Fig. 2(c)). The velocities correspond to slip velocities at the interfaces of lower permeable bed ($y = -1$) and upper permeable bed ($y = 2$). In fig. 2(d), we see that as ωt is increasing through values 0^o to 60^o, the flow velocity is increasing. Further, as ωt increases through values 60^o to 90^o, velocity decreases. Velocity profiles for different flow parameters are depicted in fig. 3. In fig. 3(a), we see that as Hartmann's number M is increasing, the velocity is decreasing. Also as Reynolds number R_1 is increasing, velocity is increasing (Fig. 3(b)). In fig. 3(c), we observe that an increase in slip parameter α results in a decrease in flow velocity. In fig. 3(d), it is noticed that as porosity parameter σ is increasing, the flow velocity is decreasing. Furthermore, in fig 3(e), it is seen that an increase in coupling parameter C_p results in an increase in flow velocity. In fig. 3(f), we see that as material parameter m is increasing, the flow velocity is decreasing.

Figures 4 and 5 depict variation in microrotation velocity for various values of governing parameter. From Figures, it is observed that microrotation velocity shows a sort of asymmetry about a plane parallel to permeable beds and nearer to upper permeable beds.

The variation in shear stress τ at the lower permeable bed (LPB) and the upper permeable bed (UPB), for different values of parameters entering into the problem is displayed through Tables. 1-8. In Table 1, we have presented the shear stress as R_1 is increasing for the fixed set of other values of parameters. As R_1 is increasing, the shear stress at both permeable beds is increasing. At fixing R_1, As frequency parameter ωt is increasing, shear stress is increasing first and then decreasing. The limit of increment in shear stress with increment in ωt depends on the value of R_1, as we see that at $R_1 = 0.5$, shear stress is increasing for ωt= 0 to $\frac{\pi}{4}$ but for $R_1 = 0.9$, the shear stress is increasing for ωt= 0 to $\frac{\pi}{2}$. In Table 2, we see that as Hartmann's number M is increasing, shear stress is decreasing at both the permeable beds. At fixing M, as frequency parameter ωt increases through values 0 to $\frac{\pi}{4}$, shear stress increases at both permeable beds and further increase in ωt results in decrease in shear stress.

Table 3 shows the variation of shear stress with slip parameter α. As α is increasing, the shear stress at both permeable beds is increasing. At fixing α, as ωt increases, the shear stress at both permeable beds first increases then decreases. From Table 4, we observe that for $\omega t = 0, \frac{\pi}{4}, \frac{\pi}{2}$ as microrotation parameter P_j is increasing, shear stress at the lower permeable plate is increasing while shear stress at the upper permeable plate is decreasing. But for $\omega t = \frac{3\pi}{4}$ as P_j increases through values 1 to 5, shear stress at lower permeable bed decreases and a further increase in P_j results in a decrease in shear stress at the lower permeable bed. In Table 5, we have presented

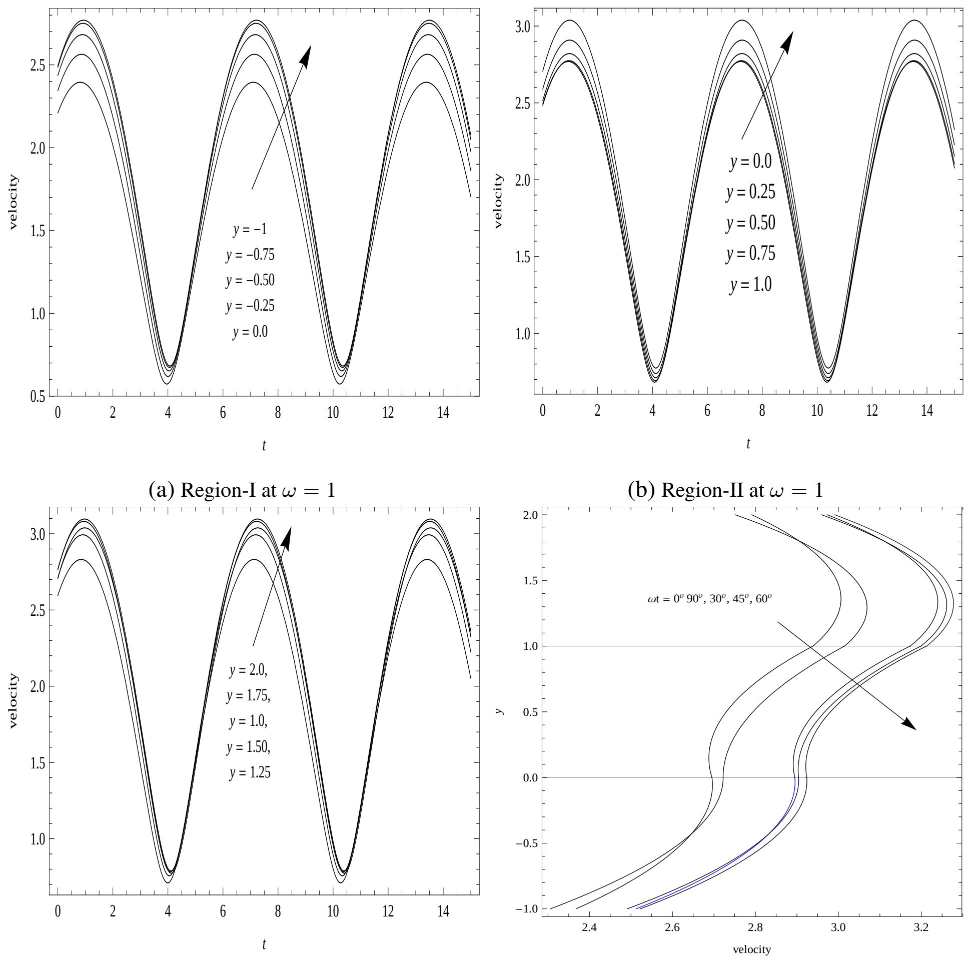

(a) Region-I at $\omega = 1$ (b) Region-II at $\omega = 1$

(c) Region-III at $\omega = 1$ (d) Frequency parameter ωt.

Figure 2: Velocity profiles with time and frequency parameter for $\rho = 1, \rho' = 1, \mu = 1.2, \mu' = 0.8, R_1 = 0.5, P_s = 1, P_o = 1, \alpha = 0.5, \sigma = 1, M = 0.75, C_p = 1, n = 0.5, m = 0.5, P_j = 1, \omega = 1$ except where they are variable.

the variation of shear stress with porosity parameter σ. For $\omega t = 0, \frac{\pi}{4}$ as σ is increasing, shear stress at both permeable beds is increasing. For $\omega t = \frac{\pi}{2}$ as σ is increasing through values 1 to 3, shear stress at the lower permeable bed in increasing and a further increase in σ results in a decrease in shear stress. While at the upper permeable bed as σ increases, shear stress increases. For $\omega t = \frac{3\pi}{4}$, as σ is increasing through values 1 to 3, shear stress at both permeable bed is decreasing.

Table 6 shows that as material parameter m in increasing, shear stress at lower permeable bed is increasing while shear stress at the upper permeable plate is decreasing. In Table 7, we see that as gyration parameter n is increasing, shear stress at lower permeable bed is increasing while shear stress at the upper permeable bed in decreasing. In Table 8, we notice that as coupling parameter C_p is increasing, shear stress at both permeable beds in decreasing.

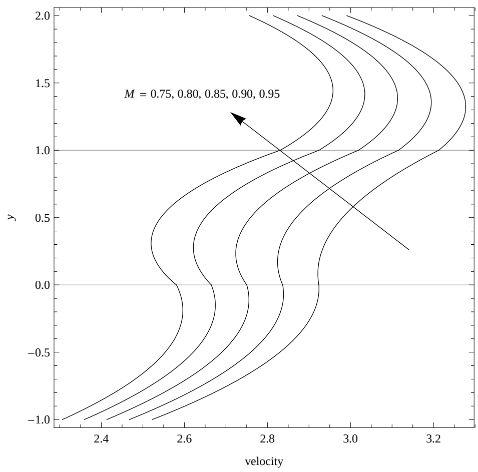

(a) Hartmann number M

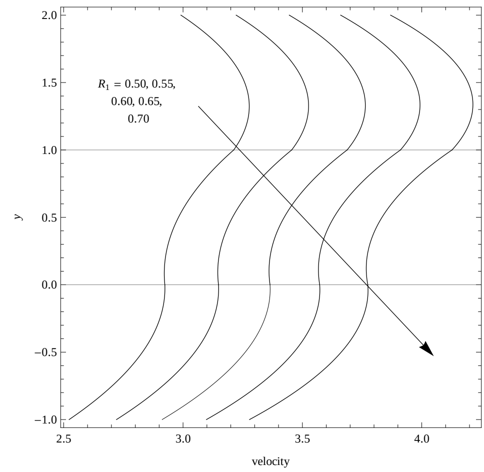

(b) Reynolds number R_1

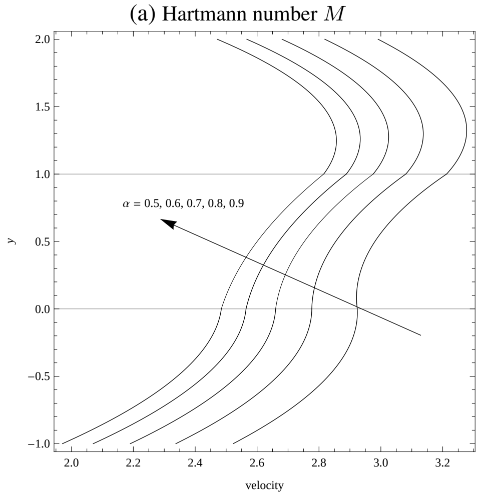

(c) Slip parameter α

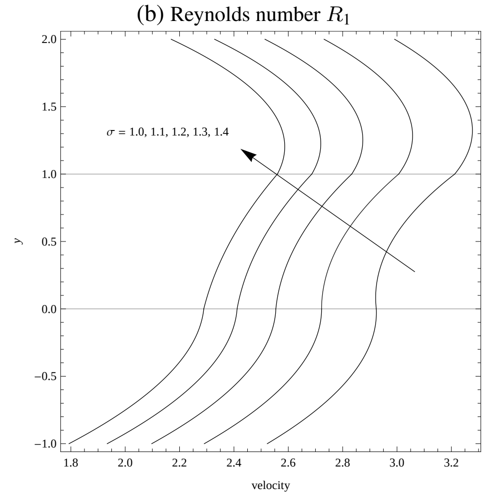

(d) Porosity parameter σ

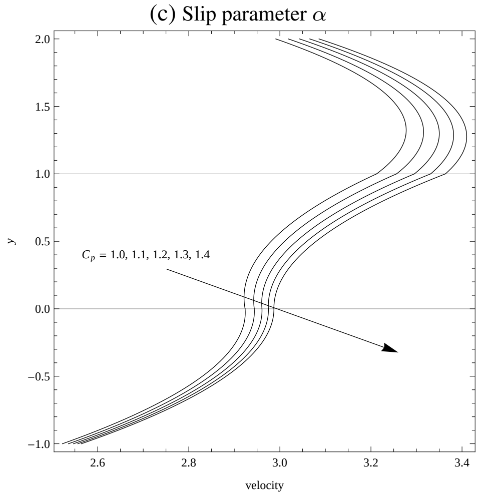

(e) Coupling parameter C_p

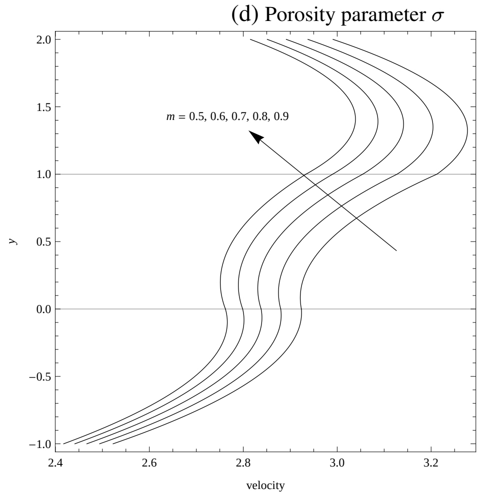

(f) Material parameter m

Figure 3: Velocity profiles for different flow parameters at $\rho = 1, \rho' = 1, \mu = 1.2, \mu' = 0.8, R_1 = 0.5, P_s = 1, P_o = 1, \alpha = 0.5, \sigma = 1, M = 0.75, C_p = 1, n = 0.5, m = 0.5, P_j = 1, \omega t = \frac{\pi}{4}$ except where they are variable.

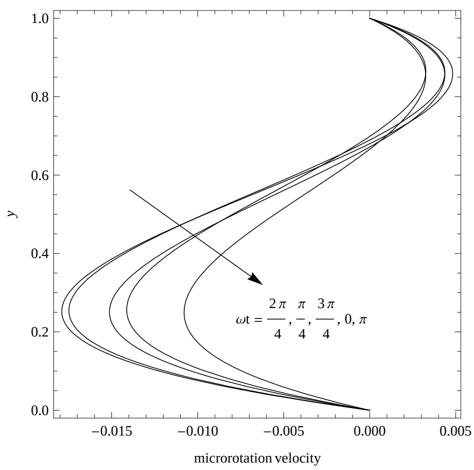

(a) Frequency parameter ωt

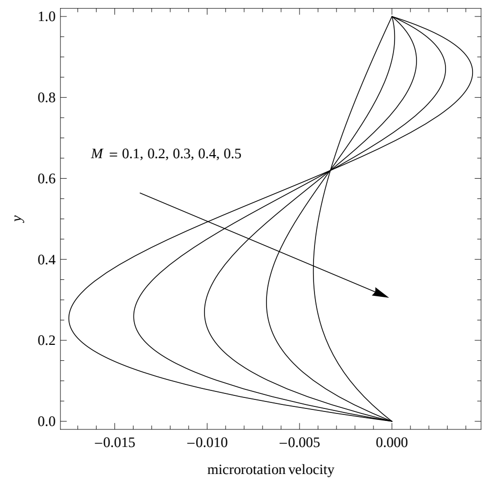

(b) Hartmann number M

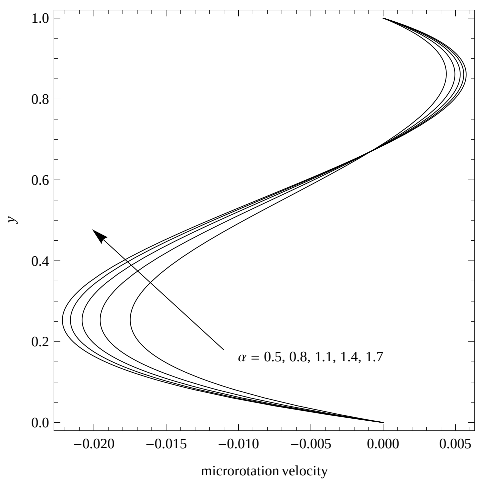

(c) Slip parameter α

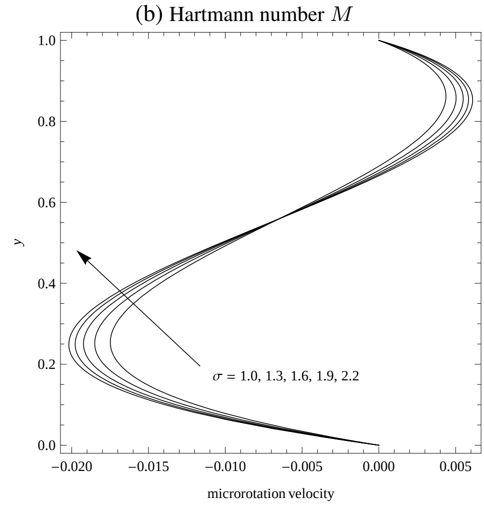

(d) Porosity parameter σ

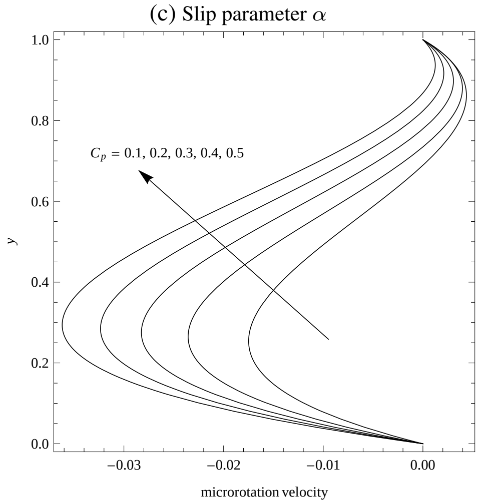

(e) Coupling parameter C_p

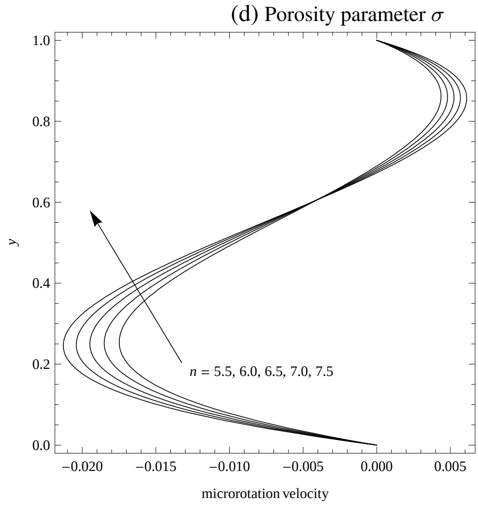

(f) Gyration parameter n

Figure 4: Microrotation velocity profile for different flow parameters at $\rho = 1, \rho' = 1, \mu = 1.2, \mu' = 0.9, R_1 = 0.2, P_s = 1, P_o = 1, \alpha = 0.5, \sigma = 1, M = 0.1, C_p = 0.1, n = 5.5, m = 0.65, P_j = 1, \omega t = \frac{\pi}{4}$ except where they are variable.

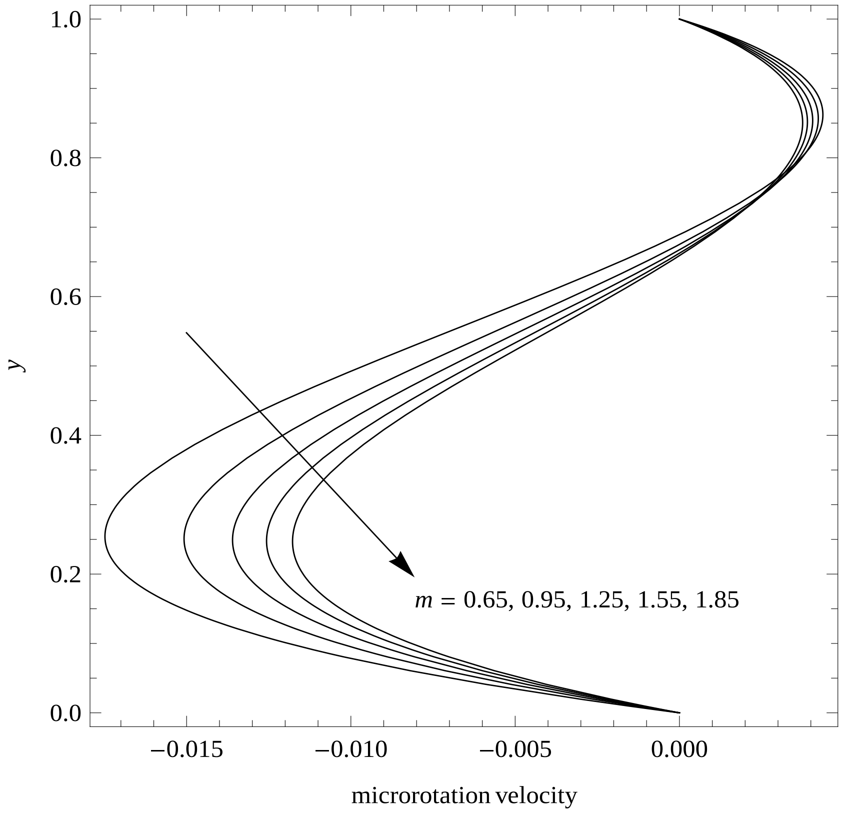

Figure 5: Microrotation velocity profile for Material parameter m at $\rho = 1, \rho' = 1, \mu = 1.2, \mu' = 0.9, R_1 = 0.2, P_s = 1, P_o = 1, \alpha = 0.5, \sigma = 1, M = 0.1, C_p = 0.1, n = 5.5, P_j = 1, \omega t = \frac{\pi}{4}$

Table 1: Variation of shear stress with Reynolds number R_1 at $\rho = 1, \rho' = 1, \mu = 1.2, \mu' = 0.8, \sigma = 1, \alpha = 0.5, M = 0.5, m = 0.5, n = 0.5, C_p = 1.0, P_s = 1, P_j = 1, P_o = 1$.

	$mod\tau$	$R_1 = 0.5$	$R_1 = 0.7$	$R_1 = 0.9$	$R_1 = 1.1$	$R_1 = 1.3$
$\omega t = 0$	LPB	0.97926	1.21428	1.41280	1.59601	1.77336
	UPB	1.08253	1.31809	1.50839	1.68158	1.85067
$\omega t = \frac{\pi}{4}$	LPB	1.08192	1.39971	1.67658	1.93081	2.17236
	UPB	1.22710	1.57439	1.87031	2.13868	2.39278
$\omega t = \frac{\pi}{2}$	LPB	1.02350	1.38391	1.71106	2.0172	2.31028
	UPB	1.18887	1.60445	1.97759	2.32418	2.65483
$\omega t = \frac{3\pi}{4}$	LPB	0.81365	1.16975	1.50929	1.83594	2.15371
	UPB	0.97412	1.40285	1.80884	2.19689	2.57266

Table 2: Variation of shear stress with Hartmann number M at $\rho = 1, \rho' = 1, \mu = 1.2, \mu' = 0.8, \sigma = 1, \alpha = 0.5, R_1 = 0.5, m = 0.5, n = 0.5, C_p = 1.0, P_s = 1, P_j = 1, P_o = 1$.

	$mod\tau$	$M = 0.5$	$M = 1.0$	$M = 1.5$	$M = 2.0$	$M = 2.5$
$\omega t = 0$	LPB	0.97926	0.783931	0.604217	0.473898	0.385319
	UPB	1.08253	0.867084	0.668042	0.523257	0.424812
$\omega t = \frac{\pi}{4}$	LPB	1.08192	0.843177	0.034012	0.489142	0.393864
	UPB	1.22710	0.958170	0.721701	0.557485	0.449426
$\omega t = \frac{\pi}{2}$	LPB	1.0235	0.775083	0.567510	0.429968	0.342458
	UPB	1.18887	0.904444	0.665684	0.506867	0.405621
$\omega t = \frac{3\pi}{4}$	LPB	0.81365	0.590353	0.414936	0.305413	0.238932
	UPB	0.97412	0.714312	0.50858	0.379119	0.300063

Table 3: Variation of shear stress with slip parameter α at $\rho = 1, \rho' = 1, \mu = 1.2, \mu' = 0.8, \sigma = 1, R_1 = 0.5, M = 0.5, m = 0.5, n = 0.5, C_p = 1.0, P_s = 1, P_j = 1, P_o = 1$.

	$mod\tau$	$\alpha = 0.1$	$\alpha = 0.2$	$\alpha = 0.3$	$\alpha = 0.4$	$\alpha = 0.5$
$\omega t = 0$	LPB	0.553001	0.724261	0.839241	0.920593	0.979268
	UPB	0.564619	0.758238	0.898184	1.00311	1.08253
$\omega t = \frac{\pi}{4}$	LPB	0.643132	0.841283	0.95758	1.03206	1.08192
	UPB	0.668034	0.901741	1.05124	1.15396	1.22710
$\omega t = \frac{\pi}{2}$	LPB	0.664281	0.846199	0.939152	0.991931	1.02350
	UPB	0.701261	0.925805	1.05437	1.13529	1.18887
$\omega t = \frac{3\pi}{4}$	LPB	0.610382	0.737959	0.787365	0.807091	0.81365
	UPB	0.654698	0.825288	0.907008	0.950289	0.97412

Table 4: Variation of shear stress with Microrotation parameter P_j at $\rho = 1, \rho' = 1, \mu = 1.2, \mu' = 0.8, \sigma = 1, \alpha = 0.5, M = 0.5, m = 0.5, n = 0.5, C_p = 1.0, P_s = 1, R_1 = 0.5, P_o = 1$.

	$mod\tau$	$P_j = 1$	$P_j = 5$	$P_j = 10$	$P_j = 15$	$P_j = 20$
$\omega t = 0$	LPB	0.979268	0.979372	0.979495	0.979588	0.979649
	UPB	1.08253	1.08240	1.08226	1.08216	1.08210
$\omega t = \frac{\pi}{4}$	LPB	1.08192	1.08210	1.08211	1.08222	1.08230
	UPB	1.22710	1.22699	1.22684	1.22672	1.22603
$\omega t = \frac{\pi}{2}$	LPB	1.02350	1.02354	1.02363	1.02372	1.02380
	UPB	1.18887	1.18880	1.18868	1.18856	1.18846
$\omega t = \frac{3\pi}{4}$	LPB	0.813651	0.813693	0.813671	0.813743	0.813813
	UPB	0.97412	0.974107	0.97404	0.973946	0.973852

Table 5: Variation of shear stress with Porosity parameter σ at $\rho = 1, \rho' = 1, \mu = 1.2, \mu' = 0.8, \alpha = 0.5, R_1 = 0.5, M = 0.5, m = 0.5, n = 0.5, C_p = 1.0, P_s = 1, P_j = 1, P_o = 1$.

	$mod\tau$	$\sigma = 1$	$\sigma = 3$	$\sigma = 5$	$\sigma = 7$	$\sigma = 9$
$\omega t = 0$	LPB	0.828586	1.13087	1.18393	1.20364	1.21357
	UPB	0.830373	1.36724	1.48410	1.53310	1.55975
$\omega t = \frac{\pi}{4}$	LPB	0.985887	1.16739	1.19000	1.19609	1.19835
	UPB	1.04206	1.42620	1.50574	1.53584	1.55166
$\omega t = \frac{\pi}{2}$	LPB	0.999361	1.02732	1.01541	1.00678	1.00094
	UPB	1.09980	1.27511	1.29890	1.30536	1.30773
$\omega t = \frac{3\pi}{4}$	LPB	0.866681	0.732575	0.687108	0.66478	0.651622
	UPB	0.994042	0.929162	0.895545	0.876975	0.865906

Table 6: Variation of shear stress with Material parameter m at $\rho = 1, \rho' = 1, \mu = 1.2, \mu' = 0.8, \sigma = 1, \alpha = 0.5, M = 0.5, R_1 = 0.5, n = 0.5, C_p = 1.0, P_s = 1, P_j = 1, P_o = 1$.

	$mod\tau$	$m = 0.1$	$m = 0.2$	$m = 0.3$	$m = 0.4$	$m = 0.5$
$\omega t = 0$	LPB	0.899858	0.927216	0.948088	0.965006	0.979268
	UPB	1.10717	1.09312	1.08628	1.08329	1.08253
$\omega t = \frac{\pi}{4}$	LPB	0.976527	1.01275	1.04039	1.06287	1.08192
	UPB	1.25292	1.23586	1.22859	1.22641	1.22710
$\omega t = \frac{\pi}{2}$	LPB	0.906406	0.946542	0.97719	1.0022	1.0235
	UPB	1.21175	1.19405	1.1875	118662	1.1887
$\omega t = \frac{3\pi}{4}$	LPB	0.700705	0.739294	0.768775	0.792943	0.813651
	UPB	0.990355	0.974477	0.969699	0.970431	0.97412

Table 7: Variation of shear stress with Gyration parameter n at $\rho = 1, \rho' = 1, \mu = 1.2, \mu' = 0.8, \sigma = 1, \alpha = 0.5, M = 0.5, m = 0.5, R_1 = 0.5, C_p = 1.0, P_s = 1, P_j = 1, P_o = 1$.

	$mod\tau$	$n = 0.5$	$n = 1.0$	$n = 1.5$	$n = 2.0$	$n = 2.5$
$\omega t = 0$	LPB	0.979268	0.978286	0.97741	0.976623	0.975913
	UPB	1.08253	1.08372	1.08477	1.08572	1.08657
$\omega t = \frac{\pi}{4}$	LPB	1.08192	1.08069	1.07960	1.07861	1.07773
	UPB	1.22710	1.22863	1.22999	1.23121	1.23232
$\omega t = \frac{\pi}{2}$	LPB	1.02350	1.02221	1.02105	1.02001	1.01908
	UPB	1.18887	1.19053	1.19202	1.19335	1.19455
$\omega t = \frac{3\pi}{4}$	LPB	0.813651	0.81248	0.811432	0.81049	0.809636
	UPB	0.97412	0.975685	0.977082	0.978337	0.97947

Table 8: Variation of shear stress with Coupling parameter C_p at $\rho = 1, \rho' = 1, \mu = 1.2, \mu' = 0.8, \sigma = 1, \alpha = 0.5, M = 0.5, m = 0.5, n = 0.5, R_1 = 0.5, P_s = 1, P_j = 1, P_o = 1$.

	$mod\tau$	$C_p = 0.2$	$C_p = 0.4$	$C_p = 0.6$	$C_p = 0.8$	$C_p = 1.0$
$\omega t = 0$	LPB	1.10624	1.04764	1.04764	0.994691	0.979268
	UPB	1.13062	1.0980	1.0980	1.08319	1.08253
$\omega t = \frac{\pi}{4}$	LPB	1.25528	1.17468	1.17468	1.10261	1.08192
	UPB	1.30741	1.25682	1.25682	1.22992	1.2271
$\omega t = \frac{\pi}{2}$	LPB	1.22312	1.12909	1.12909	1.04676	1.02350
	UPB	1.29476	1.23044	1.23044	1.19375	1.18887
$\omega t = \frac{3\pi}{4}$	LPB	1.01556	0.918693	0.918693	0.836418	0.813651
	UPB	1.09493	1.02333	1.02333	0.980623	0.97412

6 Conclusion

We analysed the problem of MHD pulsatile flow of a micropolar fluid sandwiched between two viscous fluids layers inside permeable beds. Separate solutions for flow velocity, microrotation, and mass fluxes are obtained using B-J slip boundary condition at the permeable beds. Analytical solutions are evaluated numerically for different values of governing parameters. Effects of flow parameters on flow velocity and microrotation are displayed graphically and variations in shear stress at both permeable walls are presented numerically through tables. We noticed the following

- Hartmann number M, slip parameter α, porosity parameter σ and material parameter m suppress the flow.
- Reynolds number R_1 and coupling parameter C_p promote the flow.
- Flow velocity shows mixed trends with frequency parameter ωt.
- Microrotation velocity shows a sort of asymmetry about a plane parallel to permeable beds.
- Shear stress at both permeable beds increase with the increase in Reynolds number R_1 and slip parameter α while shear stress at both permeable beds decreases with increase in Hartmann number M and coupling parameter C_p.
- Shear stress at both permeable beds show mixed trends with microrotation parameter P_j, porosity parameter σ, material parameter m and gyration parameter n.

References

[1] D.P.Hochmuth and D. K. Sunada, Ground-water model of two-phase immiscible flow in coarse material, *Ground water*, 23(5)(1985), 617-626.

[2] P. Chaturani and R. P. Samy, A study of non-Newtonian aspects of blood flow through stenosed arteries and its applications in arterial diseases, *Biorheology*, 22(6)(1985), 521-531.

[3] A. R. Rao and S. Usha, Peristaltic transport of two immiscible viscous fluids in a circular tube, *J. Fluid Mech.*, 298(1995), 271-285.

[4] M. Sharan and A. S. Popel, A two-phase model for flow of blood in narrow tubes with increased effective viscosity near the wall, *Biorheology*, 38(5,6)(2001), 415-428.

[5] A. E. Garcia and D. N. Riahi, Two phase blood flow and heat transfer in an inclined stenosed artery with or without a catheter, *Int. J. Fluid Mech. Res.*, 41(1)(2014), 16-30.

[6] K. Vajravelu, P. V. Arunachalam and S. Sreenadh, Unsteady flow of two immiscible conducting fluids between two permeable beds, *J.Math. Anal. and Appl.*, 196(3)(1995), 1105-1116.

[7] K. Vajravelu, K. Ramesh, S. Sreenadh and P.V. Arunachalam, Pulsatile flow between permeable beds, *Int. J. Non-Linear Mech.*, 38(7)(2003), 999-1005.

[8] B. G. Prasad and A. Kumar, Flow of a hydromagnetic fluid through porous media between permeable beds under exponentially decaying pressure gradient, Comput. Methods Sci. Technol., 17(1)(2011), 63-74.

[9] D. Jogie and B. Bhatt , Flow of immiscible fluids in a naturally permeable channel, *International Journal of Pure and Applied Mathematics*, 78(3)(2012), 435-449.

[10] J. Srinivas and J. V. R. Murthy, Flow of two immiscible couple stress fluids between two permeable beds, *Journal of Applied Fluid Mechanics*, 9(1)(2016), 501-507.

[11] S. Panda, S. C. Martha, and A. Chakrabarti, Three layer fluid flow over a small obstruction on the bottom of a channel, *The Anziam journal*, 56(3)(2015), 248-274.

[12] J. C. Umavathi, I.C. Leu, J. P. Kumar, and D. S. Meera, Unsteady flow and heat transfer of porous media sandwiched between viscous fluids, *Appl. Math. and Mech. - Engl. Ed.*, 31(12)(2010), 1497-1516.

[13] G. S. Beavers and D. D. Joseph , Boundary conditions at naturally permeable wall, *J. Fluid Mech.*, 30(1)(1967), 197-207.

[14] J.H. Barbee, The effect of temperature on the relative viscosity of human blood, *Biorheology*, 10(1)(1973), 1-5.

[15] H.A. Barnes, The yield stress - a review or $\pi\alpha\nu\tau\alpha - \rho\epsilon l$ - everything flows?, *J. Non-Newtonian Fluid Mech.* 81(1999), 133-178.

[16] A.C. Eringen, Theory of micropolar fluids, *J. Math. Mech.*, 16(1)(1966), 1-18.

[17] A.C. Eringen, Theory of thermomicrofluids, *J. Math. Analysis Appl.*, 38(2)(1972), 480-496.

[18] J. Peddieson and R.P. McNitt, Boundary layer theory for micropolar fluid, *Recent Adv. Eng. Sci.*, 5(1970), 405-426.

[19] T. Ariman, M.A. Turk and N.D. Sylveter, Microcontinuum fluid mechanics - a review, *Int. J. Eng. Sci.*, 11(8)(1973), 905-930.

[20] G. Lukaszewicz, Micropolar fluids: theory and application, *BirkhÃd'user, Basel*, (1999).

[21] A.C. Eringen, Microcontinuum field theories. II: fluent media, *Springer, NewYork*, (2001).

[22] Kh. S. Mekheimer, Peristaltic Flow of a Magneto-Micropolar Fluid: Effect of Induced Magnetic Field, *Journal of Applied Mathematics*, 2008(2008), Article ID 570825, 23 pages.

[23] Bitla and Iyenger, Pulsating flow of an incompressible micropolar fluid between permeable fluids, *Nonlinear Analysis: Modelling and Control*, 18(4)(2013), 399-411.

[24] P.G. Siddhewhwar and U.S. Mahabaleshwar, Analytical solution to the MHD flow of micropolar fluid over a linear streching sheet, *Int. J. of Applied Mechanics and Engineering*, 20(2)(2015), 397-406.

[25] J.P. Kumar, J.C. Umavathi, A.J. Chamakha and I. Pop, Fully-developed free convective flow of micropolar and viscous fluids in a vertical channel, *Applied Mathematical Modelling*, 34(5)(2010), 1175-1186.

[26] S. Rawat, K. Kapoor and R. Bhargava, MHD flow heat and mass transfer of micropolar fluid over a nonlinear stretching sheet with variable micro-inertia density, heat flux and chemical reaction in a non-Darcy porous medium, *Journal of Applied Fluid Mechanics*, 9(1)(2016), 321-331.

[27] J.C. Umavathi, A.J. Chamakha and M. shekhar, Flow and heat transfer of two micropolar fluids separated by a viscous fluid layer, *International Journal of Microscale and Nanoscale Thermal and Fluid Transport Phenomena*, 5(1)(2014), 23-49.

[28] J. C. Umavathi, J.P. Kumar and A.J. Chamakha, Flow and heat transfer of a micropolar fluid sandwiched between viscous fluid layers,*Can. J. Phys.*, 86(8)(2008), 961-973.

Author information

Manju Agarwal and Deepak Kumar*, Dept. of Mathematics and Astronomy, University of Lucknow, Lucknow, India Pin-226007., India.
E-mail: deepakpatel0412@gmail.com

Received: August 28, 2017.
Accepted: June 11, 2018.